

Contents

2	1	Experimental results	2
3		<i>Diamond irradiation study</i>	
4	1.1	Measurement setup	3
5	1.1.1	Preamplifiers	3
6	1.1.2	Diamond samples	5
7	1.1.3	Readout devices	6
8	1.1.4	Setup for the efficiency study using β particles	6
9	1.1.5	α -TCT setup	7
10	1.1.6	Cryogenic α -TCT setup	7
11	1.2	Particle and photon pulses and spectra	9
12	1.2.1	Noise limitations	9
13	1.3	Radiation limitations	10
14	1.3.1	Quantifying radiation damage in diamonds	11
15	1.3.2	Long-term measurement stability	14
16	1.4	Temperature limitations	20
17	1.4.1	Temperature-variant α -TCT before irradiation	20
18	1.4.2	Temperature-variant α -TCT after irradiation	21
19	1.5	Conclusion	27

²⁰ **Chapter 1**

²¹ **Experimental results**

²² *Diamond irradiation study*

²³ This chapter contains the measurement results of data taken with diamond sensors.
²⁴ First the measurement setup is described (section 1.1). Then the measured particle
²⁵ spectra are shown in 1.2. This is followed by a study of effects of irradiation damage
²⁶ on the electrical signal of the diamond detector and its lifetime. The last section
²⁷ shows the results of the measurements of irradiated diamond samples at cryogenic
²⁸ temperatures. The aim of these studies is to find the operational limitations of dia-
²⁹ mond detectors for spectroscopy and tracking applications. The studies compare the
³⁰ experimentally acquired data with the theory from the previous chapter and define
³¹ limitations of the diamond detectors in terms of noise, radiation and temperature.

³² Diamond sensors are mainly used for two types of measurements: particle counting
³³ and spectroscopy. The first type of measurements depends on the sensor's efficiency –
³⁴ the ability to detect all or at least a known percentage of radiation quanta (particles
³⁵ or photons) that hit it. The energy of the radiation is not so important; what bears
³⁶ the information is the rate and the spatial distribution. Here the radiation does
³⁷ not necessarily stop in the bulk, but rather continues its way. In spectroscopy, on
³⁸ the other hand, the idea is that a particle stops within the sensor, depositing all
³⁹ its energy, which is then measured via the freed charge carriers. The aim of the
⁴⁰ experiments described in this chapter is to:

- ⁴¹ 1. Quantify the efficiency of the sCVD diamond in counting mode,
- ⁴² 2. Quantify the degradation of efficiency with respect to the received radiation
⁴³ dose,
- ⁴⁴ 3. Quantify the macroscopic effects on charge carrier behaviour with respect to
⁴⁵ the received radiation dose and
- ⁴⁶ 4. Define limitations for its use in spectroscopy.

⁴⁷ The results discussed here show that there are several limitations for using diamond as
⁴⁸ a measurement device. All of them need to be taken into account for the measurement

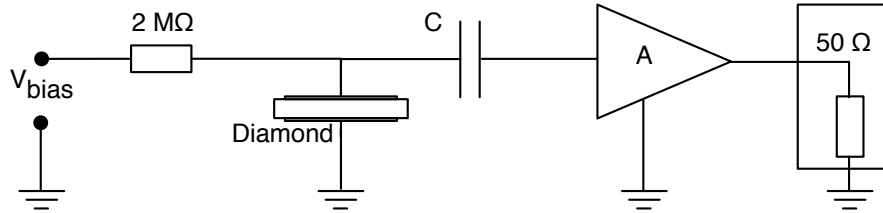


Figure 1.1: Diagram of a diamond detector readout chain.

device to perform reliably and stably. The first step is to build a setup that is insensitive to environmental interferences and minimises electrical noise in the system. The setup needs to be calibrated before use. Then, the measurement conditions have to be defined, such as the temperature, the type of radiation and its flux. This allows us to estimate the lifetime of the detector and predict the longterm change of the signal. This change can then be accounted for when interpreting the output data.

1.1 Measurement setup

To get reliable measurement results, great care has to go towards designing a measurement setup that minimises the noise in the measurements. Shielding has to be applied wherever possible. For instance, aluminium foil can be wrapped around the exposed parts of the system to shield them from external radio-frequency (RF) interferences. In addition, the sensors have to be covered to prevent the light from shining directly onto them.

The measurements using diamond that are explained in these chapters were carried out using several measurement setups, but they are all similar in terms of the electrical signal chain. The measurement chain consists of three main parts: a diamond sensor, a signal preamplifier and a readout device, as seen in diagram 1.1. The signals propagating along the analogue chain (before being digitised by the readout device) are fast – in the GHz bandwidth range – and with low amplitudes, which gives rise to importance of RF shielding. Also, the connection between the carrier and the preamplifier has to be as short as possible to avoid capacitive signal losses in the transmission line. Finally, the system needs to be grounded properly.

1.1.1 Preamplifiers

Two preamplifiers were used for the measurements, one sensitive to charge and the other to current. *CIVIDEC Cx* (figure 1.2a) is a charge shaping amplifier. Its high SNR (low noise of 400 electrons and a reported gain of ~ 8.2 mV/fC) makes it a good choice for spectroscopic measurements with diamond sensors. *CIVIDEC C2* (figure 1.2b) is a fast current preamplifier with a 2 GHz bandwidth limit. It is used for TCT measurements because of its fast response and a good SNR. Both are

1.1. MEASUREMENT SETUP

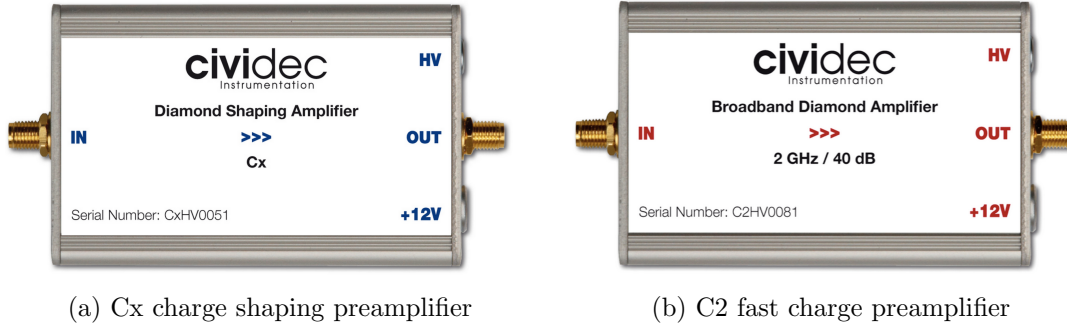


Figure 1.2: Amplifiers used for the charge and current measurements

78 embedded in an RF-tight aluminium box to reduce the noise pickup. Both have an
79 AC coupled input and an output with a $50\ \Omega$ termination.

80 **Calibration**

81 The amplifiers were calibrated before use to determine their gain. Both were cali-
82 brated using a square signal generator with a known amplitude step of $U_{\text{in}} = (252 \pm$
83 $5)$ mV. A 2 GHz oscilloscope with a 10 GS/s sampling was used to carry out these
84 measurements.

85 In the case of the Cx charge sensitive amplifier, the signal was routed through a
86 capacitor with a calibration capacitance $C_{\text{cal}} = (0.717 \pm 0.014)$ pF and then to the
87 input of the amplifier. The pulse area behind the capacitor was $a_{\text{cal}} = 5.0 \pm 0.5$ pVs
88 and the signal amplitude on the output was $U_{\text{amp}} = (1.95 \pm 0.05)$ V. The input
89 voltage step combined with the calibration capacitance yields a calibration charge
90 $Q_{\text{cal}} = C_{\text{cal}} \cdot U_{\text{in}} = (181 \pm 5)$ fC. The gain of the Cx amplifier is therefore $A_{\text{Cx}}^{\text{Q}} = \frac{U_{\text{Cx}}}{Q_{\text{cal}}} =$
91 (9.3 ± 0.4) mV/fC or $A_{\text{Cx}}^{\text{a}} = \frac{U_{\text{Cx}}}{a_{\text{cal}}} = (390 \pm 40)$ mV/pVs. The area-based amplification
92 factor has a higher uncertainty ($\sim 10\%$) than the amplitude-based factor ($\sim 4\%$)
93 due to the measurement limitations of the oscilloscope. Nevertheless, it can be used
94 as an estimate for the integrated charge of a current pulse.

95 To calibrate the C2 current amplifier, only the amplitude gain had to be measured.
96 The input signal amplitude had to be such that it kept the output amplitude within
97 the amplifier's linear range, that is ± 1 V. The signal from the generator was therefore
98 routed through a 36 dB attenuator to decrease its amplitude to $U_{\text{inAtt}} = (3.95 \pm$
99 $0.05)$ mV. Two amplifiers with different gains were measured, because both were
100 used for the measurements at different times. The output of the first amplifier was
101 $U_{\text{C2-1}} = (860 \pm 5)$ mV. This yields the amplification gain equal to $A_{\text{C2-1}} = \frac{U_{\text{inAtt}}}{U_{\text{C2-1}}} =$
102 (217 ± 3) . The second amplifier had the output equal to $U_{\text{C2-2}} = (632 \pm 5)$ mV with
103 the gain equal to $A_{\text{C2-2}} = (152 \pm 3)$.

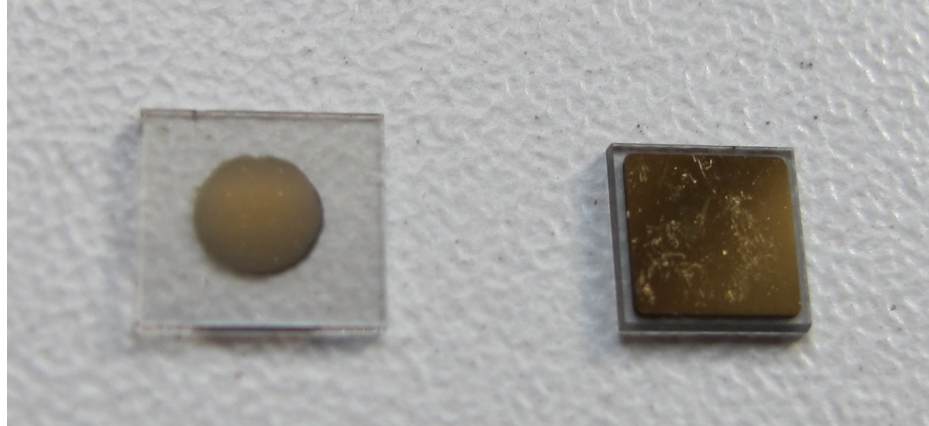


Figure 1.3: Two scCVD diamond samples: A IIa 1scdhq (left) and an E6 S37 (right)

¹⁰⁴ 1.1.2 Diamond samples

¹⁰⁵ Detector-grade diamonds are very difficult to produce, mostly because it is very dif-
¹⁰⁶ ficult to ensure a high enough purity of the lattice. It takes companies years of trials
¹⁰⁷ to produce high enough quality product. Since the target market are almost exclu-
¹⁰⁸ sively particle physics research institutes, the companies work closely with them to
¹⁰⁹ make sure the product is up to par with the requirements. All sensor samples used
¹¹⁰ to carry out these studies were bought at Element Six (E6). They all have the same
¹¹¹ standard dimensions. sCVD diamonds with dimensions $4.7 \times 4.7 \text{ mm}^2$ are already
¹¹² sufficiently large for most of the beam monitoring applications and still affordable; the
¹¹³ cost of sCVD diamonds grows exponentially with the area. There is also an ongoing
¹¹⁴ race among the producers to produce larger and larger diamonds while maintaining
¹¹⁵ the same cost. For instance, a new company IIa [] from Singapore has produced
¹¹⁶ high-quality samples with larger dimensions and the diamond detector community
¹¹⁷ is currently involved in extensive tests of their products. One of the samples with
¹¹⁸ dimensions of $5.6 \times 5.3 \text{ mm}^2$ was also sent to CERN to be characterised. The target
¹¹⁹ thickness for all the samples is $500 \mu\text{m}$. Diamonds this thick yield a high enough
¹²⁰ signal-to-noise ratio for MIPs to be measured by the electronics. Table 1.1 shows all
¹²¹ the samples used for this study. Two of them were later irradiated with 300 MeV
¹²² pions and then compared to the pre-irradiated state. Irradiation doses for damaging
¹²³ the material need to be high – above 10^{12} particles per cm^2 to be able to observe
¹²⁴ change in the sensor’s behaviour.

¹²⁵	Name	Type	Producer	Dimensions (x, y) [mm ²]	Thickness [μm]	Irradiated
	S37	sCVD	E6	4.7×4.7	548	no
	S50	sCVD	E6	4.7×4.7	537	no
¹²⁶	S52	sCVD	E6	4.7×4.7	515	$1 \times 10^{14} \pi_{300 \text{ MeV}} \text{ cm}^{-2}$
	S79	sCVD	E6	4.7×4.7	529	$3.63 \times 10^{14} \pi_{300 \text{ MeV}} \text{ cm}^{-2}$
	ELSC	sCVD	E6	4.7×4.7	491	no
	1scdhq	sCVD	IIa	5.6×5.3	460	no

1.1. MEASUREMENT SETUP

The diamond samples have quoted impurity densities of $\leq 2 \times 10^{14} \text{ cm}^{-3}$ and nitrogen incorporation of $\leq 1 \text{ ppb}$. The electrodes were added by various companies and institutes. For instance, S52 was metallised by a company DDL [] while the Physics Department of the University of Firenze, Italy metallised the S79. There are also several techniques for producing the electrodes. The DDL contacts consist of three layers: DLC (diamond-like carbon)/Pt/Au with 4/10/200 nm thicknesses, respectively. The metallisation for S79, on the other hand is made up of Cr/Au with a total thickness of $\sim 400 \text{ nm}$. The area coverage also differs from sample to sample. Diamonds must not be metallised until the very edge as the proximity of contacts with a high potential can lead to sparking. However, since only the areas not covered by the metallisation are sensitive, this effectively reduces the sensitive area of the sensors. In the diamonds used here the effective area was anywhere from 9 mm^2 to 18 mm^2 . Leakage current through the bulk was below 1 ns, but increased for the irradiated samples. The capacitance was of the order of $(2.0 \pm 0.3) \text{ pF}$.

1.1.3 Readout devices

Electrical signals in diamond detectors are in the GHz frequency range. To preserve this information, the readout device has to have a high bandwidth limit. For instance, a 250 MHz limit is enough for the spectroscopic measurements with the Cx charge amplifier, but might be insufficient for the current measurements with the C2 amplifier. Two devices were used take data shown in this chapter. The first choice was a 2 GHz LeCroy WaveRunner 204MXi-A. This specific model has a high enough limit for the fast current preamplifier signals. It offers a versatile solution for analogue signal readout – it is fast to set up and reliable. It is very convenient for use in lab tests and for experiments where small amounts of data are taken and where speed is not crucial. However, its slow acquisition speed turned out to be a bottleneck in the test beam experiment. Its initial 100 Hz readout rate decreased to a mere 20 Hz within 20 minutes, because every single trigger was saved as a separate file and the Windows operating system was not capable of handling 10000+ files in a single directory easily. This is why it was exchanged with a DRS4, an analogue readout device developed by PSI, Switzerland. This compact device is capable of recording up to four waveforms at a time at a steady rate of up to 500 Hz. Its 700 MHz bandwidth limitation was sufficient for the signal from the charge amplifier.

1.1.4 Setup for the efficiency study using β particles

The efficiency study of the diamond sensors was carried out at CERN in the North Hall test beam facility. There a straight high-energy particle beam of $\pi_{120} \text{ GeV}$ was provided to the users to calibrate their detectors. The beam had a transverse spread of $\sigma = 10 \text{ mm}$ in both axes. The particle rate was of the order of $10^4 \pi \text{ cm}^{-2} \text{ s}^{-1}$. A diamond sensor embedded in a PCB carrier was placed in the beam spot perpendicular to the beam. It was connected via an SMA connector directly to a charge amplifier (described below). The amplified signal was read out using a LeCroy oscilloscope and

a DRS4 analogue readout system (both described below). A computer was used as a controller and data storage for the readout device. A separate system was used as a reference detector. It is called the *beam telescope* and is a device used to cross-check the measurements of the devices under test (DUTs) and to carry out spatially resolved studies on the DUTs. It consists of several pixellated sensor planes placed in series, which can track a particle's trajectory with a precision of a few microns. The sensor planes are positioned in front of the DUT and behind it. Then the beam telescope acts as a trigger system – it triggers the readout of both the telescope data and DUT data when both the planes in front and behind the DUT recorded a hit by the impinging particle. A particle detected by all the planes within the DUT window and the DUT itself counts towards its efficiency whereas a hit missed by the DUT counts against it. To discard the hits missing the DUT, a region of interest (ROI) can be chosen in the beam telescope planes.

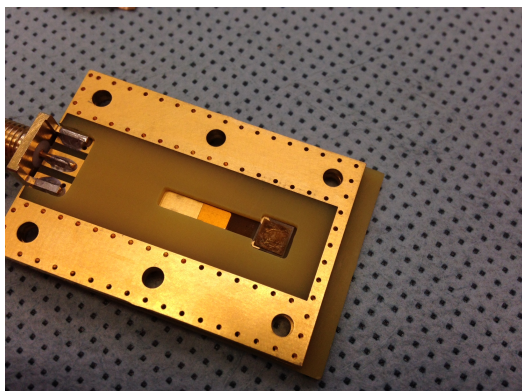
1.1.5 α -TCT setup

Room-temperature TCT measurements were carried out in the lab. The setup consisted of a diamond sensor embedded in a PCB carrier, a current amplifier and an oscilloscope. To measure α particles, their energy loss during their trajectory had to be minimised. Therefore the diamond was placed inside a vacuum chamber. The chamber was a steel tube with a diameter of 5 cm. On one side it was connected to a vacuum pump via a steel pipe. A feedthrough with an SMA connector was placed on the other side. A C2 current amplifier was connected directly onto the feedthrough. The amplified output was connected to the oscilloscope via an SMA cable. An ^{241}Am source with a diameter of 2 cm and a height of 0.5 cm was fixed onto the sensor carrier (figure 1.4a, figure 1.4b). Then the carrier was inserted in the chamber and fixed in place using an air-tight clamp. The pump was then switched on. It was capable of providing the inside pressure as low as 10^{-4} mbar after approximately one hour of operation, but measurements could take place even after five minutes of evacuation, at around 10^{-3} mbar. The most important thing to bear in mind was to switch the bias voltage of the sensor OFF during the process of evacuation, because the air becomes more conductive at the pressure of the order of 10^{-1} mbar []. A failure to switch off the bias voltage would cause a spark between the signal and ground line, destroying the amplifier.

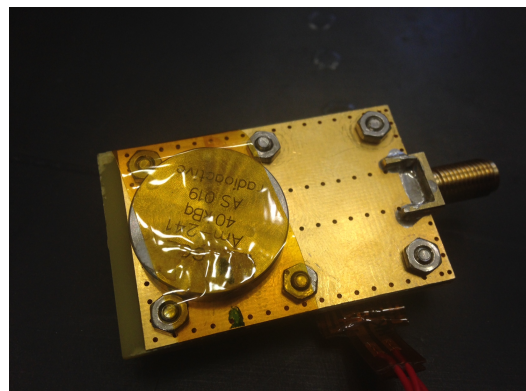
1.1.6 Cryogenic α -TCT setup

The experiment at cryogenic temperatures was carried out in the cryolab at CERN. The room-temperature TCT setup had to be modified to allow for measurements at temperatures as low as 2 K. It consisted of three parts: 1) a cryostat – a thermally insulated cylinder capable of containing liquid helium, 2) an inlet – an air-tight mechanical tube with valves and feedthroughs at the top that is lowered in the liquid helium and 3) the diamond sample, a temperature sensor, a heater and cables leading to the feedthroughs. The setup is described in detail in [].

1.1. MEASUREMENT SETUP



(a) PCB carrier with an embedded diamond sample



(b) Radioactive source over the carrier

Figure 1.4: Positioning of the α -source on top of the sensor carrier

When the diamond sample was placed in the PCB carrier and the ^{241}Am source was in place, the inlet was sealed and lowered in the empty cryostat. Then the inside volume of the inlet was evacuated to down to 10^{-5} mbar while the liquid helium was flowing into the cryostat. To improve the thermal contact between the diamond and the outside of the inlet, a small amount of helium gas was added inside the evacuated inlet, setting the vacuum to around 10^{-3} mbar. This value changed with time, because the gas condensed on the walls of the inlet, reducing the number of floating particles. For this reason the helium gas had to be added on an irregular basis. Every addition caused a significant undershoot of the sample temperature, which had to be corrected for with a heater placed on the back of the PCB carrier. Also, the added gas deteriorated the vacuum inside the inlet. It was very important to monitor the pressure so as not to let it rise above 10^{-2} mbar. The air at this pressure is significantly more conductive and could cause a short circuit between the two diamond plates or in the SMA connectors, destroying the amplifier. Furthermore, at approximately 60 K the helium gas had to be evacuated from the inlet to avoid a potential explosion due to the expansion of the gas with temperature.

When the sample was cooled to the minimum temperature achievable by use of liquid helium without over-pressurising it (4.2 K), the measurements started. After every temperature data point, the current through the heater placed in the PCB next to the diamond sample was increased, warming up the sample. The initial temperature time constant of the order of tenths of seconds at low temperatures increased with temperature and even more so when helium was evacuated from the inlet at 60 K, removing the thermal bridge between the wall of the inlet and the diamond sample. At the room temperature (RT), the time constant increased to the order of minutes.

233 **1.2 Particle and photon pulses and spectra**

234 In previous chapter the ionisation profiles for different types of radiation were dis-
235 cussed. It is known that β and γ radiation induces a triangular electric pulse whereas
236 α radiation induces a rectangular one. However, their amplitude, width and rise/fall
237 time depend heavily on the type of interaction with the diamond, the purity of the
238 diamond and the bandwidth of the amplifier and the oscilloscope. This section shows
239 the signal pulses of α , β and γ radiation with their respective energy distributions for
240 the case of a diamond detector. Then follows a discussion of effects of noise on these
241 measurements.

242 A CIVIDEC C2 current amplifier together with the LeCroy oscilloscope (both
243 with a bandwidth limit of 2 GHz) was used to record the pulse shapes whereas the
244 Cx charge amplifier was used for area distribution measurement. A 2 GHz bandwidth
245 limit defines the minimum rising time equal to $t_r \simeq \frac{0.34}{BW} = \frac{0.34}{2 \times 10^9} = 170$ ps, therefore
246 the system is capable of measuring pulses with a minimum FWHM $\simeq 170$ ps. This
247 already makes it impossible to measure the initial peak in the α response due to the
248 two flavours of charge carriers travelling. If a charge carrier travelling through the
249 bulk takes $t_{t1} \sim 6$ ns to get to the electrode on the other side ($d_1 \sim 500$ μm), the
250 carrier with the opposite charge and a shorter path to the closer electrode – max.
251 $d_2 \sim 10$ μm – already recombines in $t_{t2} \sim \frac{d_2}{d_1} t_{t1} = 120$ ps. This is too fast for the C2
252 amplifier or the oscilloscope to be able to observe.

253 Figure 1.5 shows a set of pulses and an averaged pulse for α , β and γ radiation as
254 measured by the non-irradiated sCVD diamond S37. α particles always produce the
255 same signal pulse, but with a high noise RMS. The averaging suppresses the noise
256 while still retaining most the information. It does, however, smear the rising and
257 falling edge, increasing the rise time. The t_r is now of the order of 0.5 ns. Both β and
258 γ pulses look similar - triangular and with a wide range of amplitudes. Here the pulse
259 count is low, so the pulses in the high range were not recorded, because they are very
260 rare. A trigger set very high would be needed to “catch” them with the oscilloscope.

261 **1.2.1 Noise limitations**

262 Noise is a major limiting factor in particle detection. It defines the minimum measur-
263 able particle energy and the minimum measurement resolution. It is hence important
264 to minimise the electric noise in the detector signal. The major noise contribution
265 comes from poor shielding from external electromagnetic sources. These often cause
266 ringing, whereby the signal oscillates with a frequency defined by the external source.
267 The ringing makes high-frequency measurements impossible. Another source of noise
268 is the sensor itself. In the case of silicon, natural light increases the number of ther-
269 mally excited free charge carriers, increasing the leakage current. This is not the
270 case for diamond, which is with its high energy band gap insensitive to visible light.
271 Nevertheless, any noise produced by the sensors is amplified by the signal amplifi-
272 ers, which add an additional noise of the analogue electrical circuit to the amplified
273 signal. Finally, the digitisers add the quantisation noise to the digitised signal. If

1.3. RADIATION LIMITATIONS

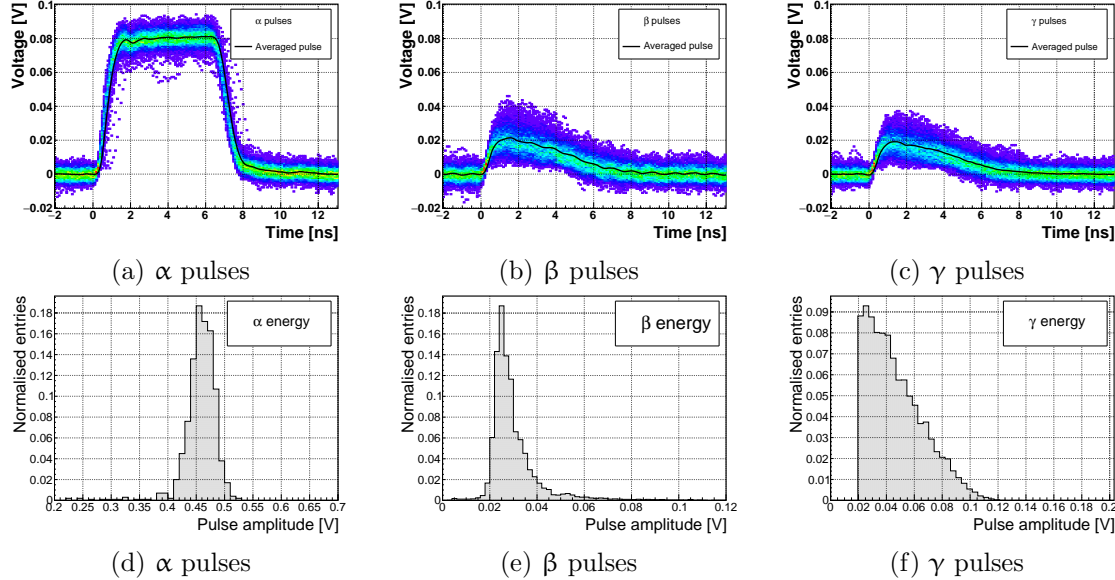


Figure 1.5: Superimposed and averaged pulses (a, b and c, current amplifier) and distributions of deposited energy (d, e, f, charge amplifier) for three types of radiation. Note the scale on the X axis of the distributions.

274 the measurement range is significantly higher than the actual measured signal, the
 275 quantisation noise can be a significant contributor to the decrease of the overall mea-
 276 surement resolution.

277 1.3 Radiation limitations

278 Exposure to ionising radiation degrades sensors. It introduces charge traps by damag-
 279 ing the sensor material. The electrons and holes created by the impinging particle get
 280 trapped in these traps, decreasing the induced current on the electrodes. This yields
 281 a lower integrated charge in an irradiated sensor than that in a non-irradiated one.
 282 Charge collection efficiency is therefore correlated with the level of irradiation. This
 283 section contains a study of the effects of pion ($\pi_{300 \text{ MeV}}$) irradiation on the charge
 284 collection efficiency of sCVD diamond detectors. To carry out this study, two di-
 285 amond samples were irradiated to $1 \times 10^{14} \pi \text{ cm}^{-2}$ (S79) and to $3.63 \times 10^{14} \pi \text{ cm}^{-2}$
 286 (S52). Then a test beam campaign was carried out to observe the charge collection
 287 efficiency at different bias voltage settings. The highest achieved efficiency values
 288 were used to determine the effective drop in efficiency with respect to received ra-
 289 diation dose. A model [] defined by a collaboration researching diamond behaviour
 290 RD42 was applied to the measured values and a damage factor was extracted. The
 291 next subsection contains measurements and results of a long-term stability study us-
 292 ing α and β particles. In particular, the charge collection efficiency as a function of
 293 time was measured during the measurements with β and α radiation. To investigate
 294 this effect on the scale of charge carriers, the change of TCT pulses with time was

295 observed. Finally, a procedure that improves the pulse shape and with it the charge
296 collection is proposed.

297 1.3.1 Quantifying radiation damage in diamonds

298 Radiation damage in semiconductors is not easy to understand and quantify. It varies
299 with the type of radiation (particles or photons) and its energy. There are several
300 models existing [?, ?, ?] that try to explain the impact of irradiation and to provide
301 *hardness factors* to compare the radiation damage between different particles. The
302 standard way is to convert the damage into *neutron equivalent*. Some models have
303 been extensively verified with simulations and with experiments. In these experiments
304 charge collection in sensors is measured before and after irradiation. This procedure
305 is repeated several times, with a measurement point taken after every irradiation.
306 When a set of measurements of charge collection is plotted against the radiation
307 dose received by a specific particle at a specific energy, a damage factor k_λ can be
308 extracted. Damage factors have to be measured across a range of energies and types
309 of radiation to properly quantify the damage in the sensors. They are then compared
310 against the simulations to verify that the experimental observations are in line with
311 the theory.

312 Radiation damage in silicon is well understood and explained. Silicon sensors
313 have a relatively low cost and are widespread. This makes irradiation studies with
314 high statistics feasible. Diamond, on the other hand, is an expensive material and
315 the technology is relatively new as compared to silicon. Therefore not many insti-
316 tutes are carrying out diamond irradiation studies. To join the efforts, the RD42
317 collaboration [] was formed. It gathers the experimental data from diamond irradia-
318 tion studies. Unlike with silicon, the experimental results so far show no significant
319 correlation with the NIEL (non-ionising energy loss) model [?], which correlates de-
320 tector efficiency with the *number of lattice displacements*. Therefore an alternative
321 model was proposed [?], correlating the diamond efficiency with *displacements per*
322 *atom* (DPA) in the bulk. Figure 1.6 shows the DPA model for a range of energies of
323 proton, pion and neutron irradiation in diamond. According to the figure, a 300 MeV
324 pion beam damages the diamond bulk twice as much as a 24 GeV proton beam. The
325 data points obtained by RD42 are also added to the figure. They have been nor-
326 malised to damage by 24 GeV protons. Finally, the data point measured in the scope
327 of this thesis has been added for comparison.

328 Irradiation with a $\pi_{300 \text{ MeV}}$ beam

329 The samples were irradiated at the Paul Scherrer Institute (PSI) [] by means of a
330 beam of pions with an energy of 300 MeV (kinetic energy 191.31 MeV) and with
331 a flux of up to $1.5 \times 10^{14} \pi \text{ cm}^{-2}$ per day. The system has a 10 % uncertainty on
332 the beam energy. In addition, due to the uncertainty on the hardness factor, the
333 equivalent fluencies have an error of $\pm 20 \%$. Looking at figure 1.6, $\pi_{300 \text{ MeV}}$ sit on a
334 steep section of the DPA distribution. After fitting a linear function to this part of

1.3. RADIATION LIMITATIONS

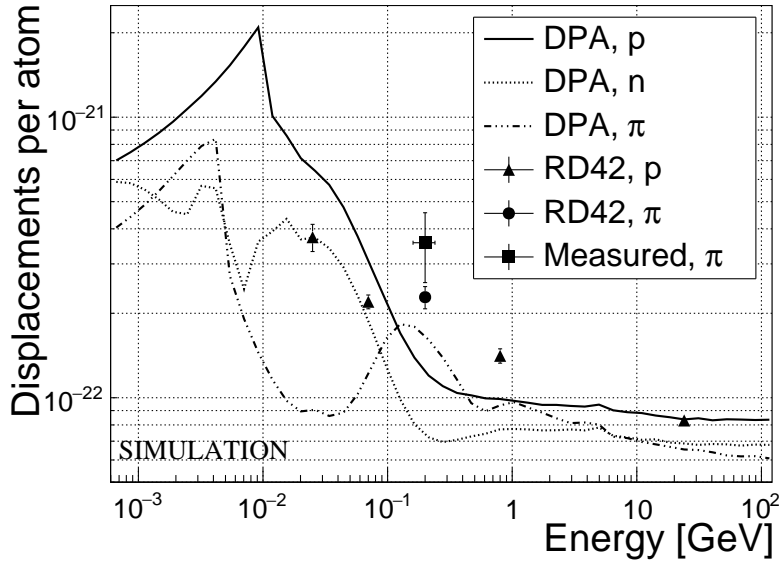


Figure 1.6: Diamond radiation damage - a model based on displacements per atom [1]. Added are data points for protons and pions by RD42 and one data point for pions measured in the scope of this thesis.

the distribution, the error on the DPA due to the uncertainty on the beam energy amounts to 7 %. Overall error on the fluency is therefore the root mean square of the uncertainty on the DPA and the uncertainty on the hardness factor: $\sigma = 21 \%$.

Two diamond samples, S52 and S79, were put in the π 300 MeV beam in the 2014 PSI irradiation campaign; S52 to $(1 \pm 0.21) \times 10^{14} \pi \text{ cm}^{-2}$ and S79 to $(3.63 \pm 0.77) \times 10^{14} \pi \text{ cm}^{-2}$. During the process, the golden electrodes got slightly activated, but the activation decayed in two weeks.

Charge collection efficiency and charge collection distance

Three diamonds – non-irradiated S37 and irradiated S52 and S79 – were tested in a $\pi_{120 \text{ GeV}}$ test beam [1] before and after irradiation. The goal was to estimate the charge collection efficiency (CCE) and charge collection distance (CCD) as a function of irradiation dose. The samples were primed (pumped) prior to data taking using a ^{90}Sr radioactive source. The data were then taken at a range of bias voltages ranging from 30 V to 900 V, yielding between $0.06 \text{ V}/\mu\text{m}$ and $1.8 \text{ V}/\mu\text{m}$ electrical field in the bulk. Every data point contained approximately 5×10^4 measured particles. The charge deposited by the particles was measured using a CIVIDEC Cx charge preamplifier. As expected, the integrated amplitude spectrum followed a Landau distribution. Its most probable value (MPV) was used to calculate the most probable collected charge Q_i :

$$Q_i [e] = Q_i [fC] \cdot 6.241 \times 10^{18} = \frac{MPV [mV]}{A [mV/fC]} \cdot 6.241 \times 10^{18} \quad (1.1)$$

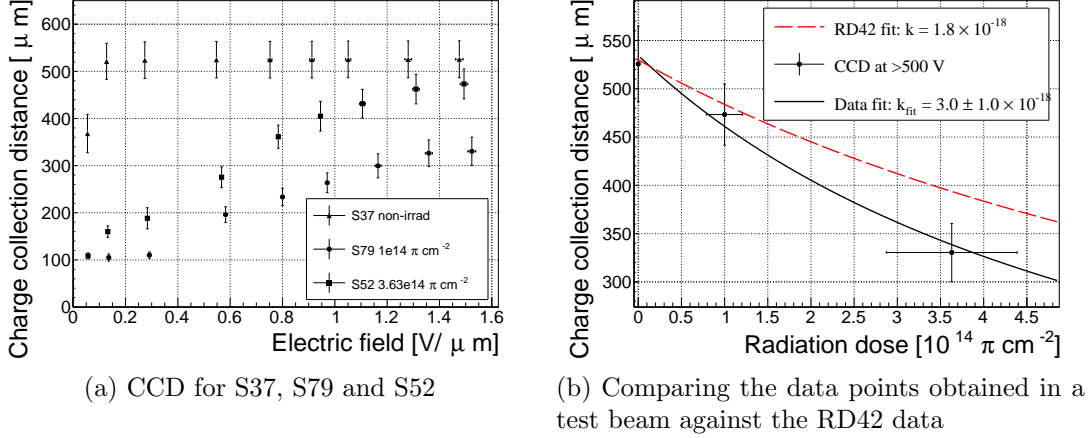


Figure 1.7: The charge collection distance at 500 V bias voltage for the three diamond samples was compared to the RD42 data for pion irradiation. The data points are about 5–15 % lower than expected from the RD42 data.

354 where $A = 9.2 \text{ mV/fC}$ is the preamplifier gain factor. The CCD was then calculated
 355 using the average number of electron-hole pairs produced per micrometer in diamond
 356 $\delta_d = 36 \text{ e-h } \mu\text{m}^{-1}$ (from table ??):

$$CCD = \frac{Q_i}{\delta d} \quad (1.2)$$

357 The resulting CCD for the three measured samples at bias voltages ranging from
 358 $0.2\text{--}1.6 \text{ V } \mu\text{m}^{-1}$ is shown in figure 1.7a. S37 exhibits full collection distance already
 359 at $0.4 \text{ V } \mu\text{m}^{-1}$ whereas the irradiated samples have a more gentle increase of CCD
 360 with increasing bias voltage. It is evident that at $1 \text{ V } \mu\text{m}^{-1}$ the maximum CCD has
 361 not been reached in the case of S79 and S52.

362 Irradiation damage factor

363 The irradiation damage factor k is a way to quantify irradiation damage of a specific
 364 particle at a specific energy. Via this factor different types of irradiation can be
 365 compared. It is obtained experimentally by measuring the CCD of a number of
 366 samples at various irradiation steps and fitting the equation 1.4 to the data. λ is the
 367 measured CCD, λ_0 is the CCD of a non-irradiated sample and Φ the radiation dose.

$$\frac{1}{\lambda} = \frac{1}{\lambda_0} + k_\lambda \cdot \Phi \quad (1.3)$$

$$\lambda = \frac{\lambda_0}{k_\lambda \lambda_0 \Phi + 1} \quad (1.4)$$

368 The data points with the maximum CCD obtained in the test beam measurements
 369 were plotted against radiation dose received (see figure 1.7b). Equation 1.4 was fitted
 370 to the data points and a damage factor $k_\lambda = (3.0 \pm 1.0) \times 10^{-18} \text{ } \mu\text{m}^{-1} \text{ cm}^{-2}$ was
 371

1.3. RADIATION LIMITATIONS

372 obtained. This value is for a factor of two higher than the damage factor obtained by
373 RD42. A possible cause is that the irradiated samples did not yet have a full charge
374 collection at $1.5 \text{ V } \mu\text{m}^{-1}$. Also, with only two samples measured, the statistical
375 uncertainty was high. Nevertheless, it can be concluded that the 300 MeV pions
376 damage the diamond bulk more than the 24 GeV protons.

377 1.3.2 Long-term measurement stability

378 An important requirement for particle detectors is stable performance over long pe-
379 riods of time. For instance, the charge collection for a defined type and quantity of
380 radiation must not change over time or has to change in a predicted way. Diamonds
381 are stable as long as their environment and their operating point does not change
382 significantly. The stability of diamond detectors depends on many external factors.
383 The aim is to study the behaviour of diamond under controlled conditions, with the
384 goal to understand its limitations. One of these limitations is for sure the received
385 radiation dose. It might affect the long-term stability of the sensor during operation.

386 The three diamond samples (S37, S79 and S52) were exposed to two different types
387 of ionising radiation for a longer period to see if their behaviour changes over time.
388 Two parameters were observed in particular: 1) charge collection of β particles and
389 2) charge collection and ionisation profile of α particles. The results showed in both
390 cases that priming plays an important role in diamond measurement stability. The
391 β particles have a “healing” effect on the diamond; MIP detection is therefore rather
392 stable in the long run, despite the fact that the sensors had been degraded by means
393 of irradiation. Alpha particles, on the other hand, deteriorate the measurement,
394 probably by introducing space charge into the sensor bulk.

395 β long-term stability

396 The samples were intentionally not primed before the measurements took place. The
397 same initial conditions are usually found in HEP experiments. The measurement
398 setup consisted of a diamond sample with the Cx spectroscopic amplifier, a silicon
399 diode with a C6 amplifier for a trigger and a ^{90}Sr source on top. A particle emitted by
400 the source traversed the sensor bulk and hit the silicon diode, triggering the analogue
401 signal readout. The source was left on the top for the course of the experiment.
402 The measurements, however, took place at discrete times. For every data point,
403 approximately 10^4 triggers were recorded. The offline analysis of the recorded signal
404 pulse amplitudes yielded a landau distribution for every data point. The resulting
405 graph of charge collection over time (see figure 1.8) shows that the charge collection
406 efficiency improves over time when the diamond sensor is primed with a β source.
407 This is especially evident in the case of the two irradiated samples. S79 achieves close
408 to full efficiency whereas S52 reaches about 50 %. Both increases are significant.
409 After approximately 30 minutes the signal stabilises. As expected, the signal of the
410 non-irradiated S37 did not change with time – this pure sCVD diamond sample had
411 the maximum collection distance from the start.

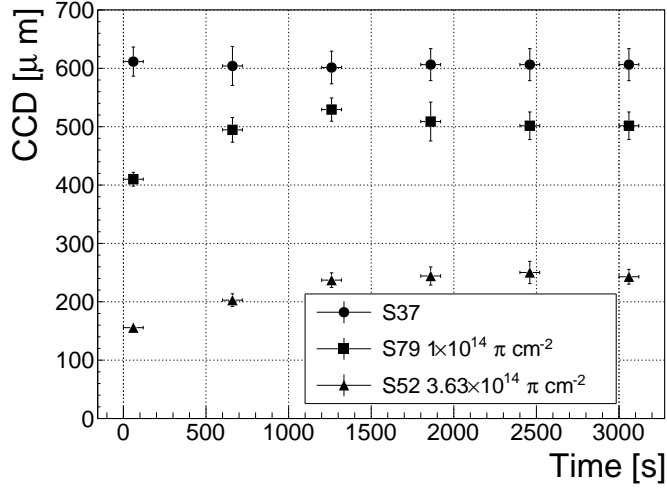


Figure 1.8: Increase of charge collection over time due to priming with the ^{90}Sr radioactive source

412 It should be noted that the ~ 2.28 MeV electrons emitted by this source are not
 413 MIPs; their charge deposition is higher than that of an electron MIP, according to
 414 the Bethe-Bloch distribution [1]. Nevertheless, for the purpose of these measurements
 415 this energy was adequate since only the relative change in charge collection was of
 416 our interest.

417 To sum up, diamond is a good choice for β radiation detection. Even if damaged by
 418 radiation, it reaches a stable charge collection in the order of an hour. The efficiency
 419 decreases with received radiation dose, but the decrease can be accounted for if the
 420 damage factor and the rate energy of the particles are known. γ radiation has a
 421 similar impact on the diamond as the β . The impinging photons, if they interact
 422 with the diamond, prime the bulk, causing the increase in charge collection efficiency.
 423 The difference, however, is in the interaction probability (cross section), which is
 424 several orders of magnitude lower for gammas.

425 α long-term stability

426 This part discusses the stability of irradiated diamond sensors during α measurements.
 427 It is safe to assume that they will behave differently than when subject to β radiation.
 428 This is due to the point-like charge carrier creation when an α particle impinges the
 429 bulk. The energy is approximately 20 times higher than the most probable value
 430 of a MIP; deposited in a small volume, it will behave differently to the track-like
 431 energy deposition of MIPs. In addition, carriers of only one polarity drift through
 432 the sensor while the others almost instantly recombine with the adjacent electrode.
 433 Taking into account that the diamond bulk has been damaged by irradiation, these
 434 two phenomena might have an effect on the operation of the detector on a macro
 435 scale.

1.3. RADIATION LIMITATIONS

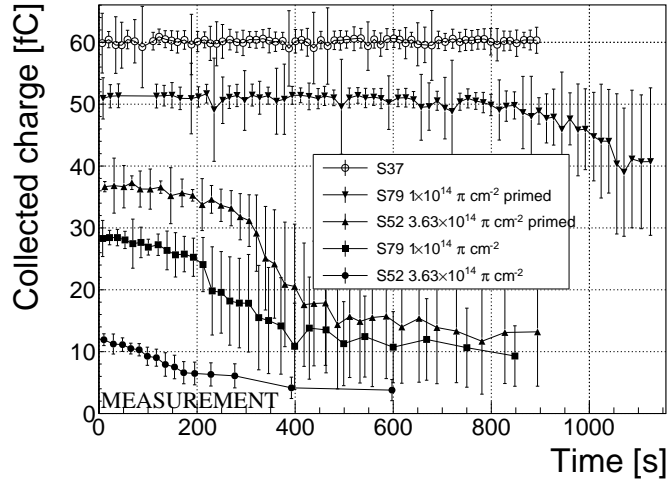


Figure 1.9: Comparison of collected charge with time for non-irradiated and irradiated diamond samples.

The measurement setup consisted of a PCB carrier for a diamond with a fitted ^{241}Am source and a vacuum chamber. The carrier was placed into the chamber, which was then evacuated. It acted as shielding for external noise pickup and ensured that the α particles didn't lose energy traveling through air. An SMA feedthrough ensured the electrical connection to the outside. The samples were measured before and after priming, at both polarities, to compare the behaviour of both electrons and holes as charge carriers. The scope of the measurements was to observe the changes in charge collection efficiency and/or in the pulse shapes.

The first test was carried out using the Cx spectroscopic amplifier. The bias voltage of the samples was set to +500 V and the signals from the diamond were measured for \sim 15 minutes. Figure 1.9 shows the results of these measurements. The collected charge for the non-irradiated sample was stable with time. It was expected that the irradiated samples will have a lower charge collection efficiency than the non-irradiated sample. However, their initial efficiency suddenly dropped after a certain period of time. The initial efficiency was improved after priming, but eventually it deteriorated again. In addition, the spread of measured energies increased significantly. Also, the particle counting rate decreased with the decreased efficiency.

The next step was to observe the behaviour of the current pulse shapes with time using a C2 current amplifier. The shape of the pulse holds more information about the charge carrier properties in the sensor than solely the value of the integrated charge. This time only the primed S79 sample was tested. Both hole and electron collection were observed to determine whether they behave differently or not. The sample was measured long enough for the pulse shapes to start changing. The data in figures 1.10 show that the initially stable pulses start deteriorating – suddenly there are several different shapes, some still the same as at the beginning while the others with almost zero amplitude. These data are difficult to interpret. Nevertheless,

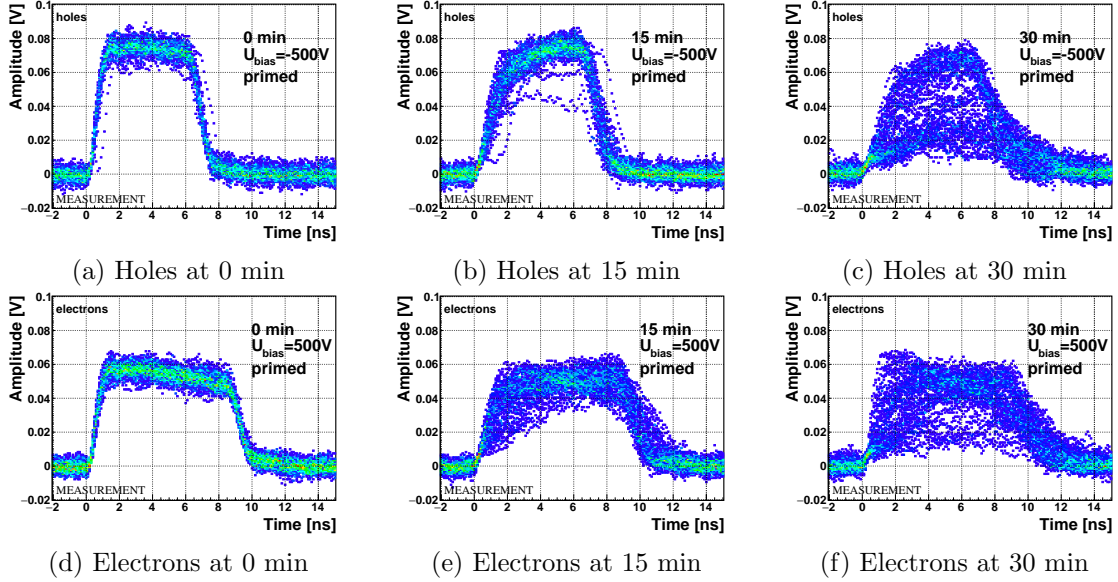


Figure 1.10: The signal of the irradiated and primed S79 deteriorates with time for both polarities. Every plot contains 60 superimposed pulses.

the idea is that some charges get trapped in the charge traps in the bulk for a long time, building up regions of space charge. Since only one charge flavour is drifting through the bulk whereas the other is quickly recombined, this already determines the imbalance in spatial distribution of trapped charges. The built up space charge affects the electric field, making it non-uniform. The non-uniform field in turn affects the drifting carriers, slowing them down or speeding them up, depending on the field gradient. Since the movement of the carriers is inducing the electric current, the field gradient can be observed in the signal. Unfortunately the effects are very convoluted, probably due to the entry point of the α particle.

At the beginning of every run, 60 reference pulses of the initial pulse were taken and plotted overlapped into a 2D histogram. An average pulse was extracted from this 2D distribution. Then a reference correlation between the reference pulses and the averaged pulse σ_{ref} was calculated. Subsequent data points also consisted of a set of 60 pulses. At every data point the correlation with the initial averaged pulse σ was calculated. From the ratio between the initial correlation σ_{ref} and discrete correlation values σ in time, the shape correlation $\text{Corr}_{\text{shape}}$ was calculated:

$$\text{Corr}_{\text{shape}}(t) = \frac{\sigma_{\text{ref}}}{\sigma} = \frac{\sum_x \sum_y w_{\text{ref}} \cdot (y_{\text{avg}} - y_{\text{ref}})^2}{\sum_x \sum_y w \cdot (y_{\text{avg}} - y)^2}, \quad (1.5)$$

where y_{avg} is the amplitude of the current averaged pulse at time x , y_{ref} is the amplitude of the initial averaged pulse at time x , y is the amplitude of the superimposed pulses in the 2D histogram and w and w_{ref} are weights for the superimposed pulses for the current data point and the initial data point.

Figure 1.11 shows the resulting time-resolved shape correlations. From the data obtained it can be concluded initial pulse shape quickly starts deteriorating. In fact,

1.3. RADIATION LIMITATIONS

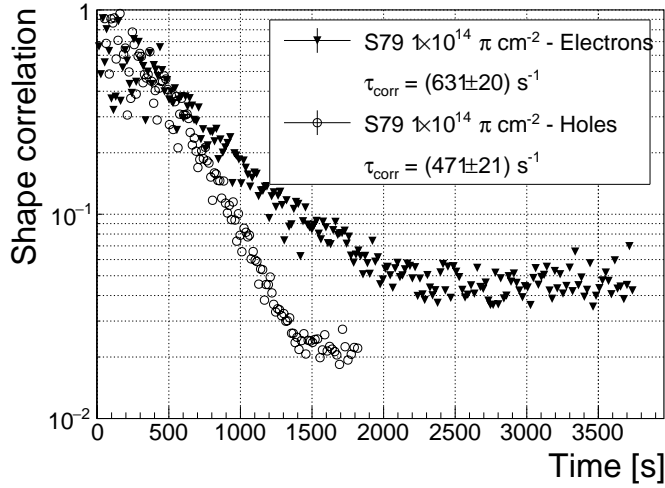


Figure 1.11: Deterioration of the pulse correlation with time

484 the deterioration of the shape correlation follows an exponential decay function, which
 485 was fitted to the data. The resulting decay constants for electrons and holes are
 486 $\tau_{\text{corr}_e} = (631 \pm 20) \text{ s}^{-1}$ and $\tau_{\text{corr}_h} = (471 \pm 21) \text{ s}^{-1}$. The electrons seem to retain the
 487 initial shape for longer. The deteriorated shapes also seem to be for a factor of 2
 488 better than those of the holes.

489 Finally, an effort has made to find a way for the pulse shapes to return to their
 490 initial state. Five methods were tested:

- 491 1. Removing the source and leaving the bias voltage switched on,
- 492 2. Removing the source and switching the bias voltage off,
- 493 3. Priming with γ without bias voltage,
- 494 4. Priming with β with bias voltage switched on and
- 495 5. Priming with β without bias voltage.

496 The diamond sample S79 was first primed using a ^{90}Sr source for about one hour.
 497 Then the bias voltage was switched on and an ^{241}Am source was put on top. The
 498 pulses produced by the impinging α particles had a proper rectangular pulse at the
 499 beginning, but then started changing in an erratic way, as described in the text above.
 500 After approximately 30 minutes, one of the methods was tested. When a “healing”
 501 procedure was started, a set of 60 pulses was taken at irregular points of time to
 502 observe the change in the pulse shape and to assess the quality of the “healing”
 503 procedure. Then the bias voltage was switched off and the sample was primed again
 504 to reset its state before starting with the next run.

505 It turns out that the methods (3) and (5) improve the shape, method (2) helps
 506 slowly, (1) does not show any change with time and (4) at first improves, but then
 507 significantly degrades the shape. The effect observed in method (4) has already been

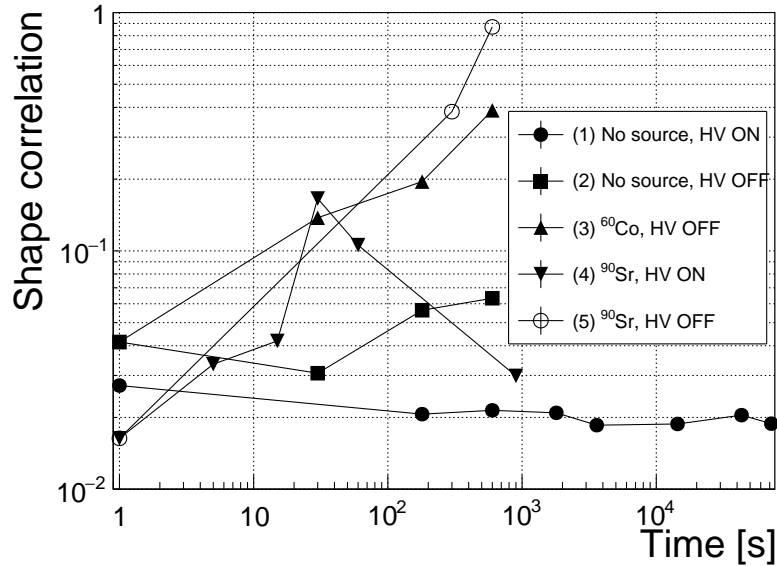


Figure 1.12: Five procedures of the “healing” process for an irradiated diamond that was exposed to α radiation at bias voltage switched on for at least 30 minutes.

described in [?]. The “healing” process therefore depends on the rate of radiation, the bias voltage and the time of exposure. The ionising radiation creates free charges, which quickly recombine close to the place of generation. It is likely that they also release the charges trapped during the measurement, reducing the overall effect of the space charge. The traps get filled with both flavours of carriers, thus they are neutralised. The pulse shape gradually returns to its initial state.

Procedure	Source	Bias voltage	Effectiveness
1	/	ON	no
2	/	/	slow
3	^{60}Co	/	YES
4	^{90}Sr	ON	no
5	^{90}Sr	/	YES

Table 1.2: Effectiveness of healing procedures

In summary, the shape of the pulses caused by α radiation changes with time for irradiated samples. The shape of the pulses gets distorted and becomes erratic. Charge collection decreases and its spread increases. This happens even faster for non-primed diamonds. To “heal” the diamond – to bring the pulse shapes back to their initial shape – the sample must be primed using a β or a γ source for several minutes at the bias voltage set to 0 V. Switching to the inverse polarity for a few seconds helps a bit, but in a long run distorts the signal, which cannot get back to its initial shape.

524 1.4 Temperature limitations

525 A test was carried out to evaluate the effect of temperature changes on the output
526 signal of the diamond sensors. A cryostat filled with liquid helium was used to
527 cool down the sensor during the measurement process. The current signal response
528 to α -particles was measured at 18 temperature points between 4 K and 295 K. At
529 every temperature point, a set of 300 pulses was read out at various bias voltages.
530 Resulting data showed that the charge collection is stable down to 150 K, where it
531 starts decreasing and stabilises again at about one third of the initial value at 75 K.
532 This behaviour was first measured and discussed by H. Jansen [?].

533 The band gap energy in diamond is equal to $E_g = 5.5$ eV while the average energy
534 to produce an electron-hole pair is $E_{e-h} = 13.25$ eV. This means there is excessive en-
535 ergy deposited in the diamond bulk. The impinging α -particle stops within $\sim 10 \mu\text{m}$
536 of the bulk, transferring all its energy to the lattice. A part of this energy, approxi-
537 mately 40 %, directly ionises the carbon atoms, creating free electron-hole pairs. The
538 remaining energy, however, is converted into lattice vibrations (phonons [?]). This
539 means that the lattice within the ionisation volume (approximately $\sim 10 \mu\text{m} \times \sim 2 \text{ nm}$
540 in size) is briefly heated up. The hot plasma then cools down to the temperature of
541 the surrounding material by heat dissipation, (i.e. phonon transport).

542 The positively charged hole and negatively charged electron in the hole attract
543 each other via the Coulomb force and may undergo a bonding process during which
544 a phonon is emitted. That phonon is referred to as *exciton* [?]. The electron is
545 pushed to a exciton energy band, which is 80 meV under the conduction band. At
546 higher temperatures, the lattice provides enough energy to excite the electron from
547 the exciton state back to the valence band (*exciton recombination* []). At lower
548 temperatures, however, the exciton lifetime increases, which means that it will take a
549 longer time for the electrons to get re-excited to the valence band. The re-excitation
550 lifetime at room temperature is ~ 30 ps, increasing to $\sim 150 \mu\text{s}$ at 50 K.

551 1.4.1 Temperature-variant α -TCT before irradiation

552 Three sCVD diamond samples were tested at a range of temperatures using the
553 α -TCT technique. At each temperature point, the bias voltage was set to several
554 positive and negative values. A set of 300 pulses was recorded at every data point
555 and averaged offline. The resulting averaged pulses of sample S37 at the 260 K
556 temperature point and a bias voltage of ± 400 V, ± 500 V and ± 700 V are shown in
557 figure 1.13. The pulses induced by holes as charge carriers are shorter than those
558 induced by electrons, which means that holes travel faster in diamond. The area of
559 the pulse, however, is the same for both polarities, which corresponds to the fact that
560 the same amount of charges is drifting in both cases.

561 Figure 1.14 shows pulses at a bias voltage set to ± 500 V across the range of
562 temperatures between 4 K and 295 K – room temperature (RT). Several conclusions
563 can be drawn by observing their shape. First, the pulse shapes change with decreasing
564 temperature. The pulse time gets shorter, hinting at the faster carrier drift velocity

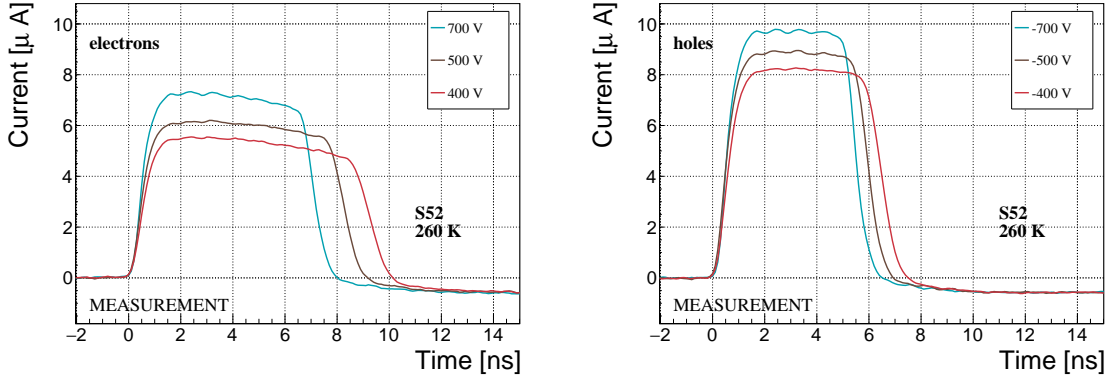


Figure 1.13: Varied bias voltage at a fixed temperature

565 v_{drift} . Second, between 150 K and 75 K there is a significant change in shape - the
 566 time constant of the rising edge increases significantly and the pulse area decreases.
 567 From 75 K down to 4 K there is no significant observable change. Last, the top of
 568 the pulse at the S52 is not flat, which means that a portion of the drifting charge is
 569 lost along its way. This could be due to impurities in the diamond bulk, which act
 570 as charge traps, or due to the space charge built up in the bulk. A linear pulse top
 571 hints on the latter. All in all, the pulse shape changes significantly with temperature,
 572 which is predicted by Jansen's model.

573 1.4.2 Temperature-variant α -TCT after irradiation

574 The irradiated S79 and S52 were re-tested in the cryostat. The aim was to see how
 575 their pulse shapes change with decreasing temperature, in particular the decaying
 576 top of the pulses (see figure 1.15). The decay time gives information on trapping of
 577 charge carriers while travelling through the diamond bulk. A variation of the decay
 578 time constant as a function of temperature might help to reveal the type and depth of
 579 the charge traps. To observe these effects or lack thereof, a number of requirements
 580 had to be met. First, the diamond samples were intentionally not primed prior
 581 to the experiment because priming would improve the pulse shapes and possibly
 582 change the decay time constant of the signal. Second, keeping in mind that the pulse
 583 shape of irradiated diamonds changes with time, the length of the measurement of an
 584 individual data point had to be short – of the order of 30 seconds. Last, the sequence
 585 of the bias voltage settings was important, the reason for which is explained below.

586 Unfortunately it was not possible to avoid temporal pulse changes. For instance,
 587 one measurement point took approximately one minute. After the measurement, the
 588 bias voltage polarity was swapped for a few seconds to bring the diamond back into its
 589 initial state. But a few seconds with respect to a minute was not enough. Therefore,
 590 when the bias voltage was set to the next value, there was still some residual effect
 591 of the previous measurement. Similar to the effects of polarisation, this effect was
 592 also decreasing the pulse height. This can be observed in figure 1.15, which shows

1.4. TEMPERATURE LIMITATIONS

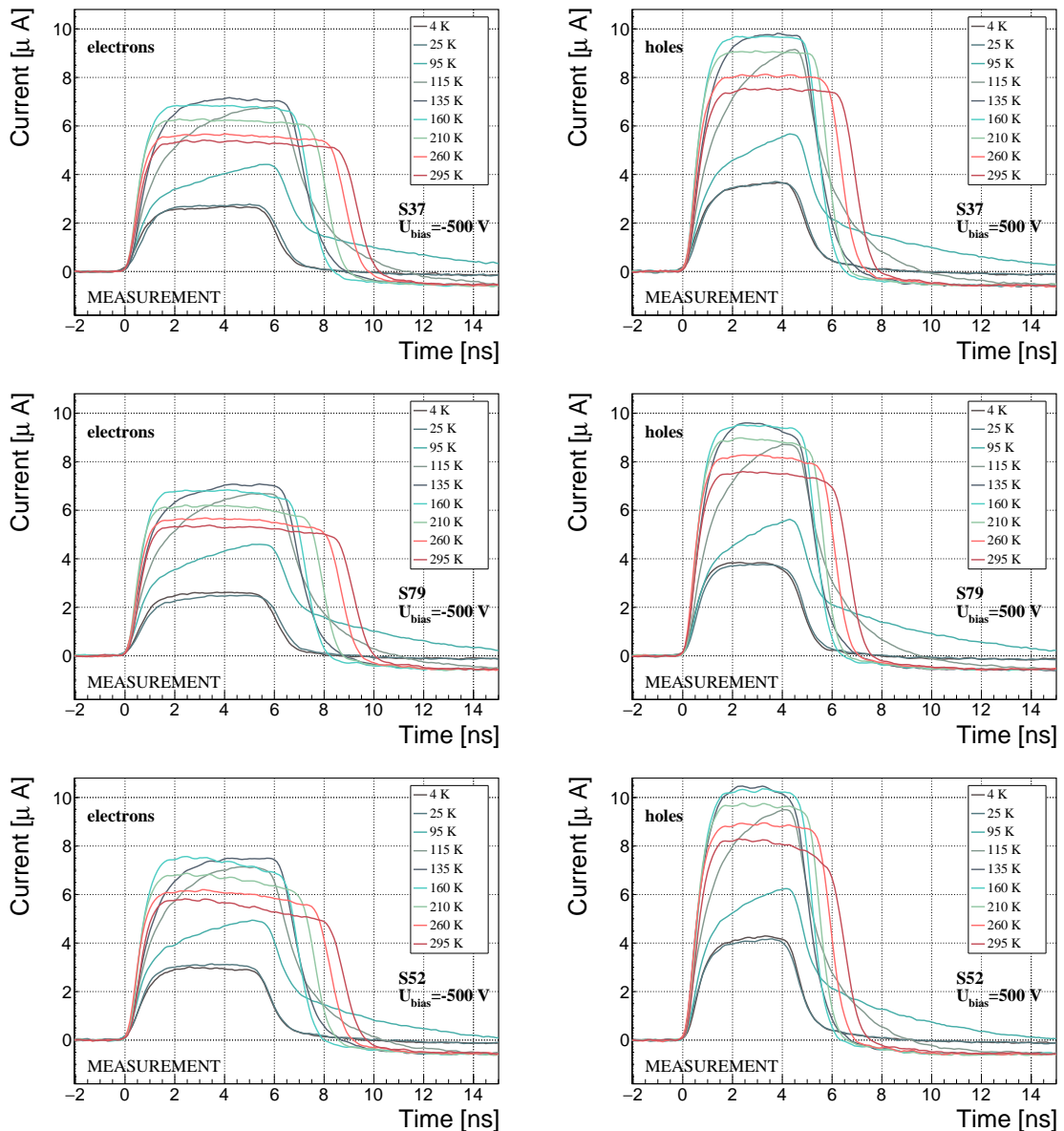


Figure 1.14: Several data points between 4 K and 295 K at a bias voltage of ± 500 V

593 the resulting pulses of S52 for bias voltages of ± 200 V, ± 300 V, ± 400 V and ± 500 V
594 at 230 K and 260 K. In this case the measurements sequence was: 230K (200 V,
595 300 V, 400 V, 500 V, -500 V, -400 V, -300 V), 260 K (-200 V, -300 V, -400 V, -
596 500 V, 500 V, 400 V, 300 V). The changes in pulse shapes for holes at 230 K and
597 260 K cannot be attributed to the temperature change. Instead, the explanation
598 could lie in diamond “polarisation”. This means that, when exposed to an electric
599 field with α measurements ongoing, the diamond builds up an internal electric field
600 of inverse polarity, which effectively reduces the overall electric field. This internal
601 field does not dissipate when the external bias voltage is switched off. It can be said
602 that the diamond becomes “polarised”. When switching the polarity of the external
603 bias voltage, the internal and external electric field point in the same direction at
604 the beginning, increasing the overall electric field and with it the pulse height. In
605 figure 1.15, this happens when switching from 500 V to -500 V at 120 K. The built up
606 polarisation contributes to the pulse having a sharp rising edge and a high amplitude.
607 This effect decays during the next two voltage points. There would be a handful of
608 ways to avoid this polarisation effect in the data:

- 609 1. After every data point invert the bias voltage and leave it to return to a neutral
610 state for the same amount of time,
- 611 2. Make a hysteresis of data points, going from minimum negative to maximum
612 positive bias several times,
- 613 3. Reduce the measurement time at every bias voltage setting.

614 Unfortunately, options (1) and (2) are very time consuming and would increase the
615 overall experiment time to over one day. The third option would worsen the resulting
616 averaged pulses. In the end an alternative option was chosen: alternating the starting
617 bias voltage and the sequence at every temperature point. With this option, the
618 highest possible systematic error in analysing the pulse shapes could be attained.

619 Figure 1.16 shows the irradiated S52 and S79 as well as the non-irradiated S37
620 for comparison, all at a bias voltage of ± 500 V and at several temperature points
621 between 4 K and RT. It is evident that the radiation damage affected the shape of
622 the pulses across all temperatures.

623 Collected charge as a function of temperature

624 The area below the current pulse is proportional to the charge collected by the di-
625 amond detector. The collected charge was observed as a function of temperature.
626 First, the amplitude values of the averaged pulses at a bias voltage of ± 500 V and
627 across the temperature range between 4 K and 295 K were integrated. Then a cal-
628 ibration factor was used to derive the charge for all data points. This factor was
629 obtained using a Cx charge-sensitive amplifier. The resulting values for electrons and
630 holes are plotted in figures 1.17a and 1.17b, respectively. This behaviour has already
631 been observed and explained in []. The new contribution are the data points for the

1.4. TEMPERATURE LIMITATIONS

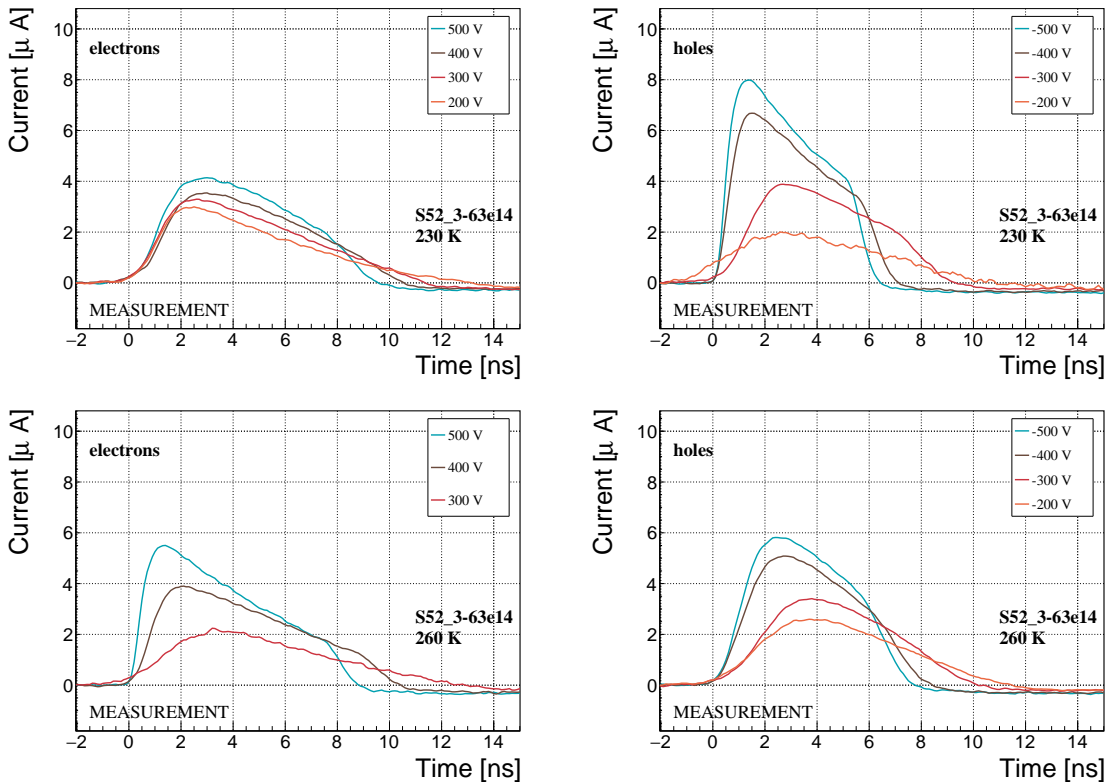


Figure 1.15: Varied bias voltage at a fixed temperature for an irradiated sample

632 irradiated samples. The values for them are lower than those of non-irradiated
633 samples, which is expected.

634 The values for all samples are fairly stable in the range between 4 K and 75 K
635 and between 150 K and 295 K. However, in the values for the irradiated S52 some
636 excursions can be observed. This is due to the sequence of the measurement steps,
637 which introduced a hysteresis effect and is explained in the preceding text.

638 The collected charge drops significantly from 150 K down to 75 K. In the non-
639 irradiated samples the values in the lower temperature range are approximately 0.30
640 of the values at the high range. For the irradiated ones this difference is lower – a
641 factor of 0.35 for S79 and 0.5 for S52. An interesting detail is that the ratio between
642 the values for non-irradiated samples and their irradiated counterparts at the lower
643 range is different than at the higher range. Looking at the values for the electron
644 collection in figure 1.17a: for S52 the lower ratio is equal to 1.28 and the higher equal
645 to 1.7. For 79 these ratios are 1.00 and 1.09, which means that the difference in charge
646 collection between 4 K and 75 K before and after irradiation is negligible.

647 Charge trapping

648 A decaying exponential function was fitted to the decaying top of the averaged pulses
649 at bias voltages of ±400 V and ±500 V across all temperatures excluding the tran-

CHAPTER 1. EXPERIMENTAL RESULTS
DIAMOND IRRADIATION STUDY

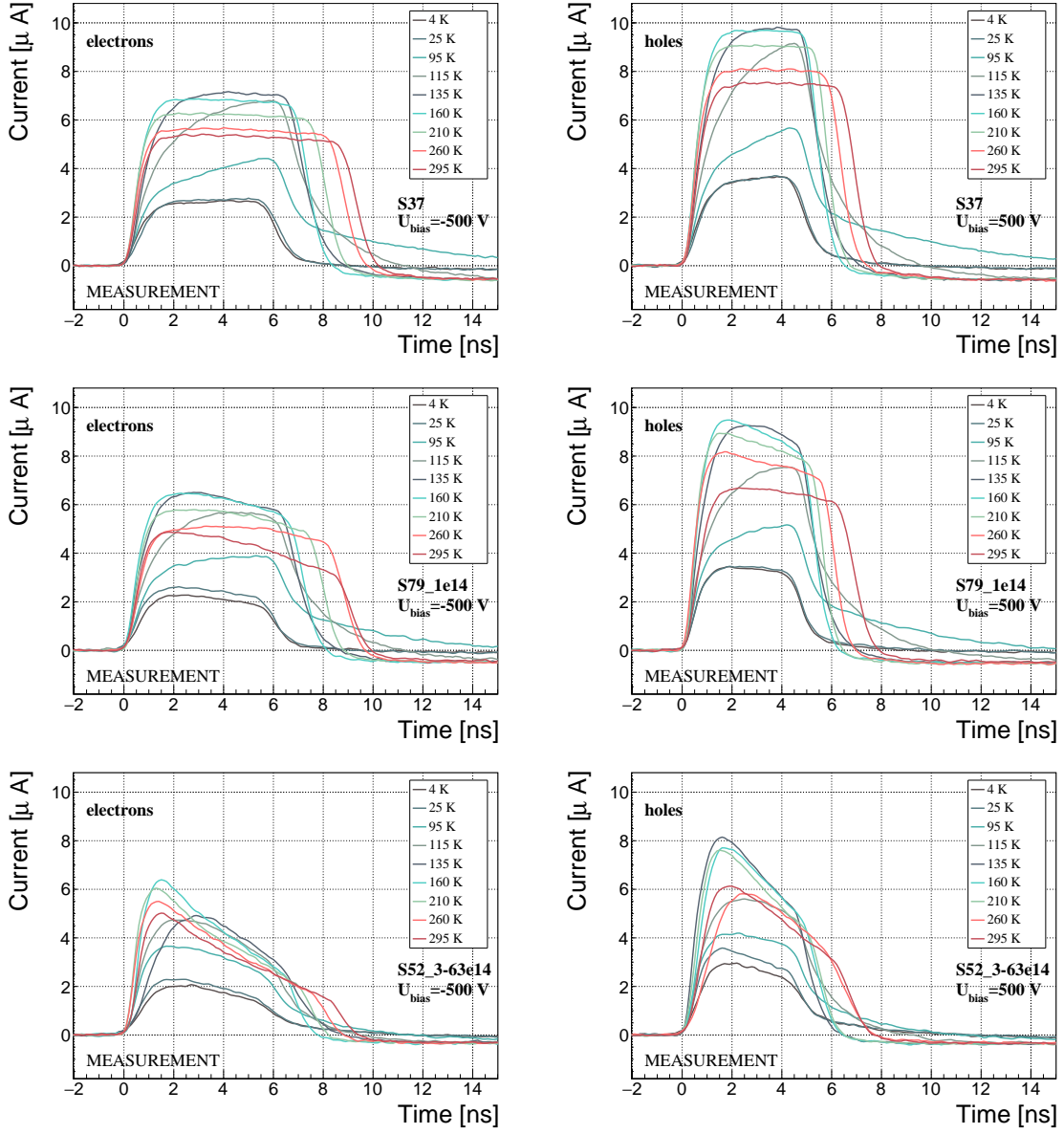


Figure 1.16: After irradiation: several data points between 4 K and 295 K at a bias voltage of ± 500 V

sitional range between 75 K and 150 K. The resulting decay time constants τ for an individual temperature point were not equal, which stems from the fact that the pulses changed with time due to “polarisation”. This counts as a systematic error. Therefore all four fitted τ were averaged into one value representing the measurement at that temperature point. Figure 1.18a shows the fitted τ for the five samples between 4 K and 295 K. In principle, the time constants should be infinite for a perfect and non-irradiated sample. Here a slightly tilted top of the pulse due to space charge was already successfully fitted with an exponential function, resulting in a τ of the order of 200 s^{-1} . This is also why the spread is large. For the irradiated samples, the

1.5. CONCLUSION

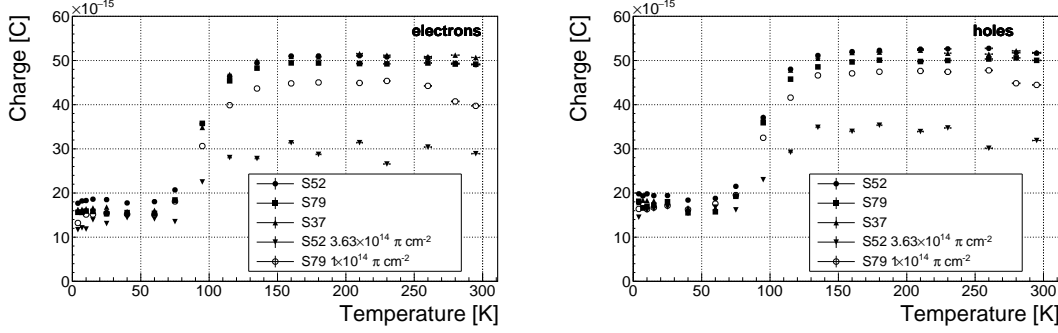


Figure 1.17: Collected charge as a function of temperature

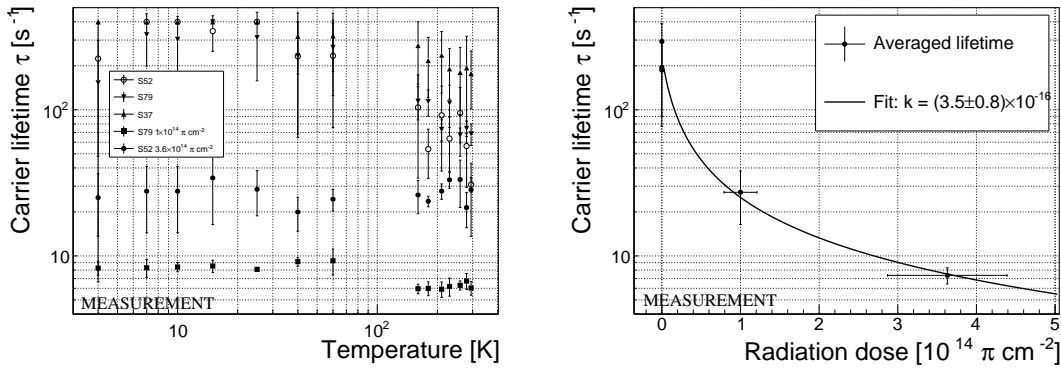
fit becomes increasingly more meaningful. As seen in figure 1.18a, the fitted values of the irradiated samples are fairly stable across all temperatures. There is a slight increase in the decay time constant of the S52 from $(6.0 \pm 0.5) \text{ s}^{-1}$ above 150 K to $(8.5 \pm 0.9) \text{ s}^{-1}$ below 75 K. On the other hand, this step is not observable in the S79 data. With only one sample exhibiting this behaviour, the effect is not significant enough. Judging by the data acquired, the samples would need to be irradiated to doses above $1 \times 10^{14} \pi \text{ cm}^{-2}$ to quantify this effect in detail. So far this effect will not be regarded as significant for the scope of this thesis. Building on this assumption, the conclusion is that the signal decay time constant for irradiated sCVD diamond is constant across the temperature range between 4 K and 195 K, excluding the transitional range between 75 K and 150 K.

Taking into account the conclusions above, all the values can be averaged into one decay constant. Figure 1.18b shows these values for all samples as a function of the received $\pi_{300 \text{ MeV}}$ radiation dose. To estimate the carrier lifetime with respect to the radiation dose received, a similar model was used than that in section 1.5. This model states that the inverse of the carrier lifetime is linearly decreasing with increasing radiation dose:

$$\frac{1}{\tau} = \frac{1}{\tau_0} + \kappa_\tau \cdot \Phi \quad (1.6)$$

$$\tau = \frac{\tau_0}{\kappa_\tau \tau_0 \Phi + 1} \quad (1.7)$$

where τ_0 is the lifetime for a non-irradiated sample (real lifetime, therefore of the order of 400 s^{-1}), τ is the lifetime of an irradiated sample, Φ is the received radiation dose and κ_τ the lifetime degradation factor. For these data the fitted factor was equal to $\kappa_\tau = (3.6 \pm 0.8) \times 10^{-16} \text{ s cm}^2 \pi_{300 \text{ MeV}}^{-1}$. Using this factor, the steepness of the decay in the pulse shape with respect to radiation dose can be estimated. This can help when designing a system where current pulse shape is an important factor.



(a) Carrier lifetime as a function of temperature

(b) Carrier lifetime averaged over all temperatures as a function of π irradiation dose

Figure 1.18: Charge carrier lifetime decreases with irradiation, but is stable across the range of temperatures between 4 K – 75 K and 150 K – 295 K.

683 1.5 Conclusion

684 This chapter gives an overview of the capabilities and limitations of diamond as
685 a particle detector. Three effects on diamond were studied – noise, radiation and
686 temperature, the focus being on the latter two.

687 Two sCVD diamond detectors were irradiated with 300 MeV pions. They were
688 tested alongside a non-irradiated sample to observe the changes in the ability to detect
689 α , β and γ radiation. Their charge collection efficiency was measured in a test beam
690 facility using . The results were compared to the results from the RD42 collaboration
691 and a DPA model []. A radiation damage factor $k_\lambda = (3.0 \pm 1.0) \times 10^{-18} \mu\text{m}^{-1} \text{ cm}^{-2}$
692 was obtained for $\pi_{300 \text{ MeV}}$ particles. The data point was not in agreement with the
693 data provided by RD42 nor with the model. However, the irradiation process and
694 the low number of tested samples hold a relatively high statistical uncertainty. In
695 addition, there was no diamond surface treatment done in between the measurements,
696 as is the case in the study conducted by RD42. The results obtained in the course
697 of these measurements will also be fed into the existing pool of data in the RD42
698 collaboration.

699 The next step was to test the long-term capabilities for α detection. The shape
700 of the ionisation profile was investigated to determine the behaviour of the charge
701 carriers in the irradiated diamond. An exponential decay was observed in the pulse,
702 proving that there are charge traps in the bulk that were created during irradiation.
703 Then a long-term stability test was carried out. The results show that the irradiated
704 diamond detectors do not provide a stable and reliable long-term measurement of α
705 particles. This might be due to a space-charge build-up in the bulk, which changes
706 the electric field, affecting the charge carriers. A procedure to improve the pulse
707 shape using β and γ radiation was proposed.

708 Finally, the diamond sensors were cooled down to temperatures between 4 K and

1.5. CONCLUSION

295 K. Their response to α particles was observed. The results of the non-irradiated and irradiated samples were compared. The effect of reduction for the number of drifting charges due to exciton recombination was observed in both sets of data. The second set had a superimposed effect of charge trapping during the drift, which was represented by an exponential decay in the signal. The decay time constant did not change with temperature. Therefore all temperature points for individual samples were averaged and the decay time constants were plotted against the received radiation dose. A damage factor equal to $\kappa_\tau = (3.6 \pm 0.8) \times 10^{-16} \text{ s cm}^2 \pi_{300 \text{ MeV}}^{-1}$ for non-primed diamonds was defined.